Analysis of the Elastic Composite in the Shape of the Human Heart

L. Jiran, T. Mares

***Abstract*—This work deals with a deformation analysis of the thick-walled closed anisotropic model whose geometry and cross-section are motivated by human heart shape. The problem is solved using the semi-analytical method, anisotropic elasticity in curvilinear coordinates and the Fourier series expansion. Several models with different geometry are briefly mentioned. The most realistic model is described in more details and its responses to the different loadings are presented.**

***Index Terms*—elasticity, tensor calculus, heart, anisotropic, analysis.**

I. Introduction

THIS report builds on the first part of the planned work to create an anisotropic model of a human heart and to determine its deformation which was described in details in [1]. In [1] there are our motivation, aims, related works and difficulties briefly discussed too. The aim of this paper is to present several elastic composite models which are used as the approximation of the real geometry of the heart. We are going to use one of this models in the next step of our work - in the future dynamic analysis. The linear elastic small deformation behavior of the modeled body is used for the analysis again.

II. Models

The heart motivated anisotropic elastic tube with a constant cross-section was used as the first model, see [1]. Models that are presented in this article are based on this first model but their geometry is more complicated to create closed model with a required cross-section - a model more similar to the real heart geometry.

We have created three different models and tested various boundary conditions. All thick-walled models are wound in six layers with the winding angle $\alpha = \pm\ \pi/6$ by a laminated composite which represents muscle mass. A static load is applied through the internal pressures.

A. Model based on the elastic tube

The first closed model was created as a modification of our previous model, see [1]. The cross-section, Fig. 1, is defined by using ellipses and circles

$$\begin{aligned} x^1 &= r_1 \xi^1 d_1 \cos\xi^2, \\ x^2 &= r_2 \xi^1 d_1 \sin\xi^2, \\ x^3 &= \xi^3, \end{aligned} \tag{1}$$

Authors are with the Department of Mechanics, Biomechanics and Mechatronics, Faculty of Mechanical Engineering, Czech Technical University in Prague, Technicka 4, 166 07 Prague 6, Czech Republic, e-mail:

$$\begin{aligned} y^1 &= \eta^1 d_2 \cos\eta^2, \\ y^2 &= \eta^1 d_2 \sin\eta^2, \\ y^3 &= \eta^3, \end{aligned} \tag{2}$$

with parameters r_1, r_2 and the range of coordinates

$$\xi^1 \in [a,b] = [1, 1.0], \xi^2 \in [0, 2\pi], \xi^3 \in [0, l] = [0, 120],$$

$$\eta^1 \in [R_1, R_2] = [15, 26.5], \eta^2 \in [0, 2\pi], \eta^3 \in [0, l] = [0, 120],$$

and

$$\begin{aligned} d_1 &= 2(-(\xi^3 - 0.6)^2 + 0.5), \\ d_2 &= 2(-(\eta^3 - 0.6)^2 + 0.5). \end{aligned}$$

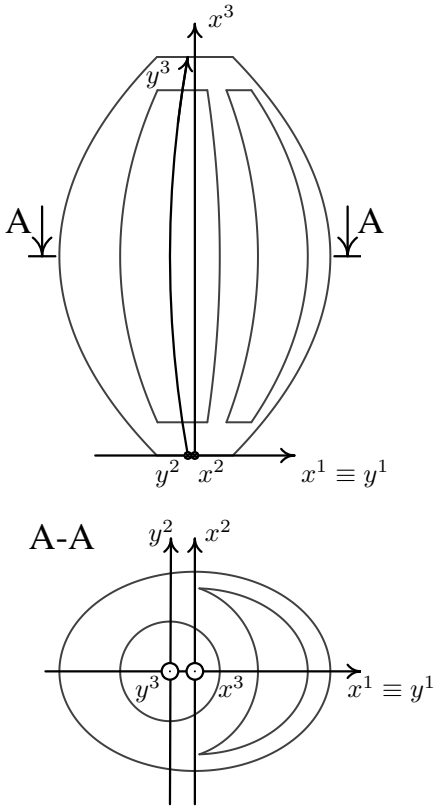

Fig. 1. The first model

B. Model based on ellipsoids

The second closed model, Fig. 2, is created via equations of two ellipsoids:

$$\begin{aligned} x^1 &= r_1\xi^1\cos\xi^2\sin(r_6\xi^3), \\ x^2 &= r_2\xi^1\sin\xi^2\sin(r_6\xi^3), \\ x^3 &= r_3 + r_4\xi^1\cos(r_6\xi^3), \end{aligned} \tag{3}$$

$$\begin{aligned} y^1 &= \eta^1\cos\eta^2\sin(r_6\eta^3), \\ y^2 &= \eta^1\sin\eta^2\sin(r_6\eta^3), \\ y^3 &= r_5 + r_4\eta^1\cos(r_6\eta^3), \end{aligned} \tag{4}$$

with parameters r_1, r_2, r_3, r_4, r_5 and the range of coordinates

$$\xi^1 \in [a,b] = [1,1.0], \xi^2 \in [0,2\pi], \xi^3 \in [0,l] = [0,120],$$

$$\eta^1 \in [R_1,R_2] = [15,26.5], \eta^2 \in [0,2\pi], \eta^3 \in [0,l] = [0,120].$$

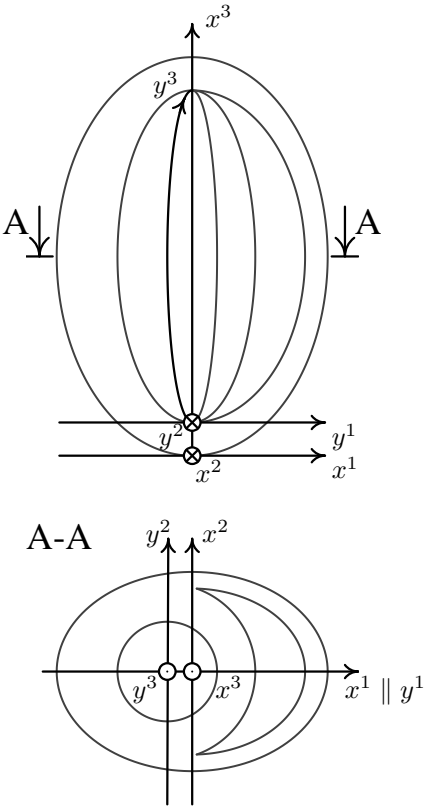

Fig. 2. The second model

C. Non-symmetric closed model

The third closed model, Fig. 3, is created via equations of two ellipsoids too but other relation between coordinate systems y^i and x^i enables us to create model whose outer profile is non symmetric. A wall thickness of the modeled left and right ventricles is approximately constant for the all height of the model (compare Fig. 2 with Fig. 3).

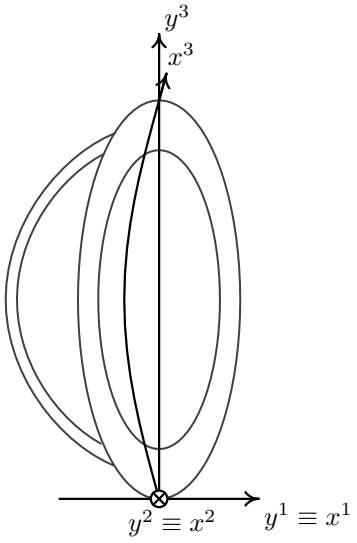

Fig. 3. The third model.

III. Non-symmetric closed model of the heart

Deformation analysis procedure is described in details only for the third of developed models which in our opinion best approximates the real heart geometry. Other two models were only briefly introduced.

We are going to use this model and apply a dynamic load, model a circulation of blood, use a viscoelastic material behavior and model active functions of heart muscles in the future work.

A. The coordinate systems

The heart geometry is modeled via two ellipsoids and there are introduced six coordinate systems for description, Fig. 4 and Fig. 5. The global Cartesian coordinate system, y^i, the global circular coordinate system, η^i, the global coordinate system, x^i, the global elliptic coordinate system, ξ^i, the local Cartesian coordinate system, μ^i, and the local Cartesian coordinate system, ν^i, aligned with the direction of the local orthotropy.

This coordinate systems are defined by the mutual relations in the next paragraphs.

The relations between the global circular coordinate system η^i and the global Cartesian coordinate system y^i are

$$\begin{aligned} y^1 &= r_5\eta^1\cos\eta^2\sin(r_6\eta^3), \\ y^2 &= r_5\eta^1\sin\eta^2\sin(r_6\eta^3), \\ y^3 &= r_3 + r_4\eta^1\cos(r_6\eta^3), \end{aligned} \tag{5}$$

where r_3, r_4, r_5, r_6 are the properly selected parameters of the ellipsoid. The coordinates η^i have the range

$$\eta^1 \in [R_1,R_2] = [0.9,1.2], \eta^2 \in [0,2\pi], \eta^3 \in [0,l] = [0,120],$$

where l is the length parameter.

The relations between the global coordinate system y^i and the global coordinate system x^i are

$$\begin{aligned} y^1 &= x^1 - k\sin(r_6 x^3), \\ y^2 &= x^2, \\ y^3 &= x^3, \end{aligned} \tag{6}$$

where k is the parameter of the coordinate systems displacement.

The relations between the global elliptic coordinate system ξ^i and the global coordinate system x^i are

$$\begin{aligned} x^1 &= r_1\xi^1\cos\xi^2\sin(r_6\xi^3), \\ x^2 &= r_2\xi^1\sin\xi^2\sin(r_6\xi^3), \\ x^3 &= r_3 + r_4\xi^1\cos(r_6\xi^3), \end{aligned} \tag{7}$$

where r_1, r_2 are the remaining parameters of the ellipsoid. The coordinates ξ^i have the range

$$\xi^1 \in [a,b] = [0.95, 1.05], \xi^2 \in [0, 2\pi], \xi^3 \in [0, l] = [0, 120].$$

The relations between the coordinate system ξ^i and the global computing coordinate system η^i are known

$$\begin{aligned} \eta^2 &= \arctan\left(\frac{r_2\xi^1\sin(r_6\xi^2)}{r_1\xi^1\cos\xi^2\sin(r_6\xi^3) - k\sin(r_6x^3)}\right) \\ \eta^3 &= \frac{1}{r_6}\arctan\left(\frac{r_2\sin\xi^2\xi^1\sin(r_6\xi^3)}{r_5\sin\eta^2\cos(r_6\xi^3)\xi^1}\right) \\ \eta^1 &= \frac{r_1\cos\xi^2\xi^1\sin(r_6\xi^3) - k\sin(r_6x^3)}{r_5\cos\eta^2\sin(r_6\eta 3)}. \end{aligned} \tag{8}$$

The coordinate systems y^i, μ^i, ν^i are Cartesian. The metrics are

$$\overset{y}{g}_{ij} = \overset{\mu}{g}_{ij} = \overset{\nu}{g}_{ij} = \delta_{ij}. \tag{9}$$

For the components of the metric tensor $\overset{\eta}{g}_{ij}$ we have

$$\overset{\eta}{g}_{ij} = \frac{\partial y^k}{\partial\eta^i}\frac{\partial y^l}{\partial\eta^j}\overset{y}{g}_{kl}, \tag{10}$$

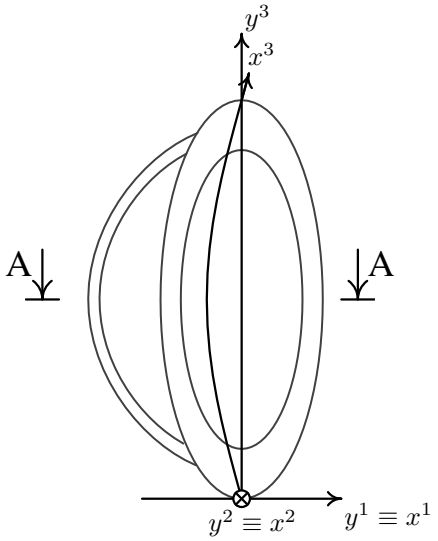

Fig. 4. The coordinate systems.

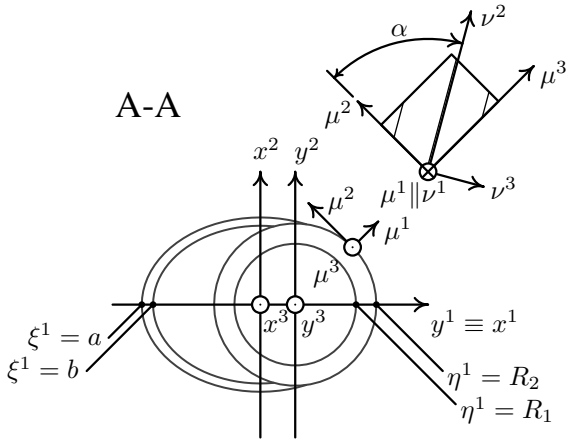

Fig. 5. The coordinate systems.

where

$$\frac{\partial y^i}{\partial\eta^j} = \begin{pmatrix} a_{11} & a_{12} & a_{13} \\ a_{21} & a_{22} & a_{23} \\ a_{31} & 0 & a_{33} \end{pmatrix}, \tag{11}$$

$$\begin{aligned} a_{11} &= r_5\sin(r_6\eta^3)\cos\eta^2, \\ a_{12} &= -r_5\eta^1\sin(r_6\eta^3)\sin\eta^2, \\ a_{13} &= \eta^1 r_5 r_6\cos(r_6\eta^3)\cos(\eta^2), \\ a_{21} &= r_5\sin(r_6\eta^3)\sin\eta^2, \\ a_{22} &= r_5\eta^1\sin(r_6\eta^3)\cos\eta^2, \\ a_{23} &= \eta^1 r_5 r_6\cos(r_6\eta^3)\sin(\eta^2), \\ a_{31} &= r_4\cos(r_6\eta^3), \\ a_{33} &= -\eta^1 r_4 r_6\sin(r_6\eta^3). \end{aligned}$$

And for the components of the metric tensor $\overset{\xi}{g}_{ij}$ we have

$$\overset{\xi}{g}_{ij} = \frac{\partial x^k}{\partial\xi^i}\frac{\partial x^l}{\partial\xi^j}\overset{x}{g}_{kl}, \tag{12}$$

where

$$\frac{\partial x^i}{\partial\xi^j} = \begin{pmatrix} b_{11} & b_{12} & b_{13} \\ b_{21} & b_{22} & b_{23} \\ b_{31} & 0 & b_{33} \end{pmatrix}, \tag{13}$$

$$\begin{aligned} b_{11} &= r_1\sin(r_6\xi^3)\cos\xi^2, \\ b_{12} &= -r_1\xi^1\sin(r_6\xi^3)\sin\xi^2, \\ b_{13} &= \xi^1 r_1 r_6\cos(r_6\xi^3)\cos(\xi^2), \\ b_{21} &= r_2\sin(r_6\xi^3)\sin\xi^2, \\ b_{22} &= r_2\xi^1\sin(r_6\xi^3)\cos\xi^2, \\ b_{23} &= \xi^1 r_2 r_6\cos(r_6\xi^3)\sin(\xi^2), \\ b_{31} &= r_4\cos(r_6\xi^3), \\ b_{33} &= -\xi^1 r_4 r_6\sin(r_6\xi^3) \end{aligned}$$

and

$$\overset{x}{g}_{ij} = \frac{\partial y^k}{\partial x^i}\frac{\partial y^l}{\partial x^j}\overset{y}{g}_{kl}, \tag{14}$$

where

$$\frac{\partial y^i}{\partial x^j} = \begin{pmatrix} 1 & 0 & -kr_6\cos(r_6x^3) \\ 0 & 1 & 0 \\ 0 & 0 & 1 \end{pmatrix}. \tag{15}$$

Others transformation matrices are

$$\frac{\partial x^i}{\partial \mu^j} = \begin{pmatrix} n_\xi^1 & -n_\xi^2 & 0 \\ n_\xi^2 & n_\xi^1 & 0 \\ 0 & 0 & 1 \end{pmatrix}, \tag{16}$$

where $\mathbf{n}_\xi = (n_\xi^1, n_\xi^2, 0)$ is the normal to the ellipse, Fig. 6, with

$$\begin{aligned} n_\xi^1 &= \frac{\frac{\partial x^2}{\partial \xi^2}}{\sqrt{\left(\frac{\partial x^1}{\partial \xi^2}\right)^2 + \left(\frac{\partial x^2}{\partial \xi^2}\right)^2}}, \\ n_\xi^2 &= \frac{-\frac{\partial x^1}{\partial \xi^2}}{\sqrt{\left(\frac{\partial x^1}{\partial \xi^2}\right)^2 + \left(\frac{\partial x^2}{\partial \xi^2}\right)^2}}, \end{aligned} \tag{17}$$

similarly

$$\frac{\partial y^i}{\partial \mu^j} = \begin{pmatrix} n_\eta^1 & -n_\eta^2 & 0 \\ n_\eta^2 & n_\eta^1 & 0 \\ 0 & 0 & 1 \end{pmatrix}, \tag{18}$$

where $\mathbf{n}_\eta = (n_\eta^1, n_\eta^2, 0)$ is the normal to the circle, Fig. 6, with

$$\begin{aligned} n_\eta^1 &= \frac{\frac{\partial y^2}{\partial \eta^2}}{\sqrt{\left(\frac{\partial y^1}{\partial \eta^2}\right)^2 + \left(\frac{\partial y^2}{\partial \eta^2}\right)^2}}, \\ n_\eta^2 &= \frac{-\frac{\partial y^1}{\partial \eta^2}}{\sqrt{\left(\frac{\partial y^1}{\partial \eta^2}\right)^2 + \left(\frac{\partial y^2}{\partial \eta^2}\right)^2}}, \end{aligned} \tag{19}$$

and finally

$$\frac{\partial \mu^i}{\partial \eta^j} = \begin{pmatrix} 1 & 0 & 0 \\ 0 & \cos\alpha & -\sin\alpha \\ 0 & \sin\alpha & \cos\alpha \end{pmatrix}, \tag{20}$$

where α is the winding angle, Fig. 5.

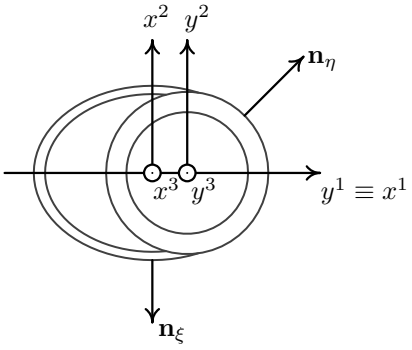

Fig. 6. Normals.

B. Deformation analysis

Deformations are determined using the principle of the total potential energy minimum. The global circular coordinate system η^i is used as the global computational coordinate system. The constrained minimum of the total potential energy is found using the Lagrange multipliers method. The necessary condition of stationary is expressed using the Lagrangian

$$\mathcal{L}(\overset{\eta}{u}_i) = \Pi(\overset{\eta}{u}_i) + L(\overset{\eta}{u}_i), \tag{21}$$

where the total potential energy of the model $\Pi(\overset{\eta}{u}_i)$ is expressed in the form

$$\Pi(\overset{\eta}{u}_i) = U(\overset{\eta}{u}_i) - W(\overset{\eta}{u}_i), \tag{22}$$

with the elastic strain energy $U(\overset{\eta}{u}_i)$ and the potential energy of the applied forces $-W(\overset{\eta}{u}_i)$. The second term $L(\overset{\eta}{u}_i)$ in (21) is the linear combination of the left-hand sides of the constrains.

1) Fourier series expansion:

The displacement functions $\overset{\eta}{u}_i$ are approximated by the Fourier series expansion and this approximation enables us to integrate the total potential energy. Fulfilment of the boundary conditions is ensured by using the method of Lagrange multipliers so the Fourier series expansion is

$$\begin{aligned} \overset{\eta}{u}_1 &= \sum_{hkm=-K}^{K} A_1^{hkm} \left(e_{hkm}\eta^1 + e_m\right), \\ \overset{\eta}{u}_2 &= \sum_{hkm=-K}^{K} A_2^{hkm} \left(e_{hkm}\eta^1 + e_m\right), \\ \overset{\eta}{u}_3 &= \sum_{hkm=-K}^{K} A_3^{hkm} \left(e_{hkm}\eta^1 + e_m\right), \end{aligned} \tag{23}$$

where A_1^{hkm}, A_2^{hkm}, A_3^{hkm} are coefficients to be determined,

$$e_{hkm} = e^{\mathrm{i}h2\pi\frac{\eta^1 - R_1}{c - R_1}} e^{\mathrm{i}k\eta^2} e^{\mathrm{i}m\eta^3 \frac{2\pi}{l}}, \tag{24}$$

and

$$e_m = e^{\mathrm{i}m\eta^3 \frac{2\pi}{l}}. \tag{25}$$

For parameter K is chosen value 3 so that each displacement function is approximated by 7^3 members of the Fourier series expansion. The coordinates ξ^i are mapped by (8) to the global computational coordinates η^i and, therefore, the coordinate η^1 has a new range $\eta^1 \in [R_1, c] = [0.9, 2.27]$. The c is the parameter in the Fourier series (23).

This mapping caused an enlargement of an area on whose is the Fourier series expansion defined, see the hatch at Fig. 7. All points of this area (described by the range of coordinates $\eta^1 \in [R_1, c], \eta^2 \in [0, 2\pi], \eta^3 \in [0, l]$) must be included in the computing procedure.

It is necessary to perform numerical integration over the whole area to obtain a numerical regularity of matrices in the calculation. Points of material which belong to the area but not to the model itself, see the hatch at Fig. 8, are considered with a minimal value of the material parameters.

2) Elastic energy:

The procedure for calculating the elastic energy U is basically the same as the procedure that was described in detail in the previous work [1]. The coordinate systems η^i is used as the computational coordinate system so we can for the elastic energy write

$$U = \frac{1}{2} A^{\mathrm{T}} K A, \tag{26}$$

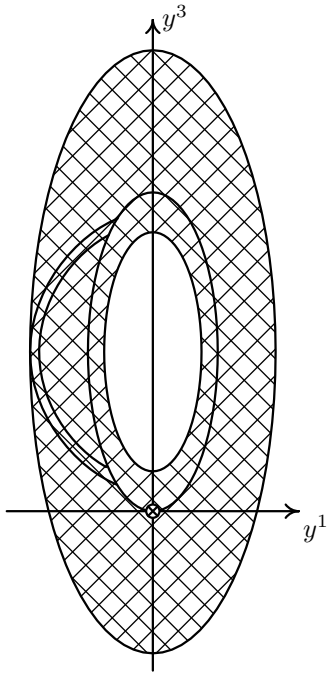

Fig. 7. The area.

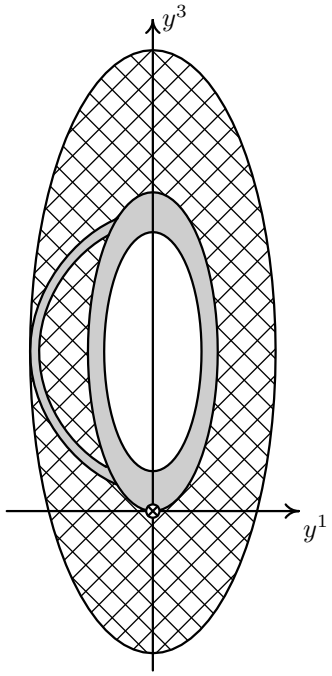

Fig. 8. The area with a minimal value of the material parameters.

where the stiffness matrix of the whole model K is a sum of $\overset{\eta}{K}$ and $\overset{\xi}{K}$

$$K = \overset{\eta}{K} + \overset{\xi}{K}, \tag{27}$$

where

$$\overset{\eta}{K} = \int_0^l \int_0^{2\pi} \int_{R_1}^{R_2} (B-G)^{\mathrm{T}} \, \overset{\eta}{E}^{ijkl} \, (B-G) \left| \overset{\eta}{g}_{ij} \right|^{\frac{1}{2}} \mathrm{d}\eta^1 \mathrm{d}\eta^2 \mathrm{d}\eta^3, \tag{28}$$

$$\overset{\xi}{K} = \int_0^l \int_0^{2\pi} \int_a^b (B-G)^{\mathrm{T}} \, \overset{\eta}{E}^{ijkl} \, (B-G) \left| \overset{\xi}{g}_{ij} \right|^{\frac{1}{2}} \mathrm{d}\xi^1 \mathrm{d}\xi^2 \mathrm{d}\xi^3, \tag{29}$$

where B and G are the matrices[1]

$$B = \begin{pmatrix} \partial v_1/\partial \eta^1 & \texttt{zeros}(1,343) & \texttt{zeros}(1,343) \\ \partial v_1/\partial \eta^2 & \texttt{zeros}(1,343) & \texttt{zeros}(1,343) \\ \partial v_1/\partial \eta^3 & \texttt{zeros}(1,343) & \texttt{zeros}(1,343) \\ \texttt{zeros}(1,343) & \partial v_2/\partial \eta^1 & \texttt{zeros}(1,343) \\ \texttt{zeros}(1,343) & \partial v_2/\partial \eta^2 & \texttt{zeros}(1,343) \\ \texttt{zeros}(1,343) & \partial v_2/\partial \eta^3 & \texttt{zeros}(1,343) \\ \texttt{zeros}(1,343) & \texttt{zeros}(1,343) & \partial v_3/\partial \eta^1 \\ \texttt{zeros}(1,343) & \texttt{zeros}(1,343) & \partial v_3/\partial \eta^2 \\ \texttt{zeros}(1,343) & \texttt{zeros}(1,343) & \partial v_3/\partial \eta^3 \end{pmatrix}, \tag{30}$$

with v_1, v_2, v_3 defined using (24) and (25)

$$v_1 = v_2 = v_3 = e_{hkm}\eta_1 + e_m, \tag{31}$$

and

$$\begin{aligned} G = &\left\{ \overset{\eta}{\Gamma}{}^1_{ij} \right\}_{ij\rceil} (v_1 \quad \texttt{zeros}(1,343) \quad \texttt{zeros}(1,343)) + \\ &+ \left\{ \overset{\eta}{\Gamma}{}^2_{ij} \right\}_{ij\rceil} (\texttt{zeros}(1,343) \quad v_2 \quad \texttt{zeros}(1,343)) + \\ &+ \left\{ \overset{\eta}{\Gamma}{}^3_{ij} \right\}_{ij\rceil} (\texttt{zeros}(1,343) \quad \texttt{zeros}(1,343) \quad v_3), \end{aligned} \tag{32}$$

where $\overset{\eta}{\Gamma}{}^1_{ij}$, $\overset{\eta}{\Gamma}{}^2_{ij}$, $\overset{\eta}{\Gamma}{}^3_{ij}$ are Christoffel symbols of the second kind.

In (28) and (29) $\overset{\eta}{g}_{ij}$ and $\overset{\xi}{g}_{ij}$ are the components of the metric tensor (10), (12) and $\overset{\eta}{E}^{ijkl}$ is the elasticity tensor in the global computational coordinate system

$$\overset{\eta}{E}^{ijkl} = \frac{\partial \eta^i}{\partial \nu^m} \frac{\partial \eta^j}{\partial \eta^n} \frac{\partial \eta^k}{\partial \nu^o} \frac{\partial \eta^l}{\partial \nu^p} \, \overset{\nu}{E}^{mnop}, \tag{33}$$

with

$$\frac{\partial \eta^i}{\partial \nu^j} = \frac{\partial \eta^i}{\partial y^k} \frac{\partial y^k}{\partial x^l} \frac{\partial x^l}{\partial \mu^m} \frac{\partial \mu^m}{\partial \nu^j}. \tag{34}$$

The elasticity tensor $\overset{\nu}{E}^{ijkl}$ in (33) in the local Cartesian coordinate system ν^i (which is aligned with the direction of the local orthotropy) is known.

Finally A in (26) is the column vector of the coefficients to be determined

$$A = \begin{pmatrix} A_1^{hkm} \\ A_2^{hkm} \\ A_3^{hkm} \end{pmatrix}. \tag{35}$$

3) Work of internal pressures:

The model is loaded by internal pressures p_1, p_2 ($p_2 > p_1$), Fig. 9. The whole procedure and all relations necessary to determining the work of the applied forces were introduced and described in previous work. See [1] for more information.

[1]Typewrite font is used for the MATLAB syntax.

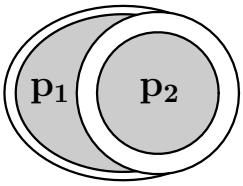

Fig. 9. Internal pressures

The procedure used in this work is quite analogous. Calculation is performed in the global computing coordinate system η^i and needed transformation matrices are described in the section *The coordinate systems*.

We can write as a result

$$W = W_1 + W_2 + W_3 = PA, \tag{36}$$

where W_1, W_2, W_3 represent works done by the pressures on the relevant surfaces.

4) Lagrange multipliers:
The method of Lagrange multipliers is used for a fulfilment of the boundary conditions. The model is fixed at three points A^η, B^η and C^η, see Fig. 10.

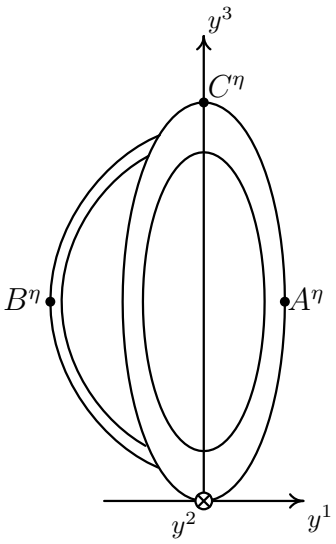

Fig. 10. The boundary conditions.

These points have in the global computational coordinate system η^i coordinates

$$\begin{aligned} A^\eta &= [\eta^1_{(A)}, \eta^2_{(A)}, \eta^3_{(A)}] = [R_2, 0, l/2], \\ B^\eta &= [\eta^1_{(B)}, \eta^2_{(B)}, \eta^3_{(B)}] = [c, \pi, l/2], \\ C^\eta &= [\eta^1_{(C)}, \eta^2_{(C)}, \eta^3_{(C)}] = [R_2, 0, l]. \end{aligned} \tag{37}$$

The point A^η is fixed in all directions $(u^\eta_1, u^\eta_2, u^\eta_3)$, the point B^η is fixed in u^η_2 and u^η_3 directions and the point C^η is fixed only in u^η_2 direction.

This condition can be written in the form

$$\begin{pmatrix} \overset{\eta}{u}_{1(A)} \\ \overset{\eta}{u}_{2(A)} \\ \overset{\eta}{u}_{3(A)} \\ \overset{\eta}{u}_{2(B)} \\ \overset{\eta}{u}_{3(B)} \\ \overset{\eta}{u}_{2(C)} \end{pmatrix} = MA = 0, \tag{38}$$

where

$$M = \begin{pmatrix} \varphi_{(\eta_A)} & \mathtt{zeros}(1,343) & \mathtt{zeros}(1,343) \\ \mathtt{zeros}(1,343) & \varphi_{(\eta_A)} & \mathtt{zeros}(1,343) \\ \mathtt{zeros}(1,343) & \mathtt{zeros}(1,343) & \varphi_{(\eta_A)} \\ \mathtt{zeros}(1,343) & \varphi_{(\eta_B)} & \mathtt{zeros}(1,343) \\ \mathtt{zeros}(1,343) & \mathtt{zeros}(1,343) & \varphi_{(\eta_B)} \\ \mathtt{zeros}(1,343) & \varphi_{(\eta_C)} & \mathtt{zeros}(1,343) \end{pmatrix}, \tag{39}$$

with

$$\varphi = e_{hkm}\eta_1 + e_m. \tag{40}$$

Then the term in (22)

$$L(\overset{\eta}{u}_i) = \lambda^T MA, \tag{41}$$

where λ is a vector of the Lagrange multipliers, matrix M is defined by (39) and A is the vector of coefficients to be determined.

5) Total potential energy:
When we use the needed relations in the form (26), (36), (41) we can write for the Lagrangian $\mathcal{L}$ (22)

$$\mathcal{L} = \frac{1}{2}A^{\mathrm{T}}KA - PA + \lambda^T MA. \tag{42}$$

The stationary condition of the Lagrangian

$$\frac{\partial \mathcal{L}}{\partial A} = KA - P + M^T\lambda = 0, \frac{\partial \mathcal{L}}{\partial \lambda} = MA = 0$$

leads to

$$\begin{pmatrix} K & M^T \\ M & \mathtt{zeros}(6,6) \end{pmatrix} \begin{pmatrix} A \\ \lambda \end{pmatrix} = \begin{pmatrix} P \\ \mathtt{zeros}(1,6) \end{pmatrix} \tag{43}$$

and the column vector A of the coefficients to be determined is realized from

$$\begin{pmatrix} A \\ \lambda \end{pmatrix} = \begin{pmatrix} K & M^T \\ M & \mathtt{zeros}(6,6) \end{pmatrix}^{-1} \begin{pmatrix} P \\ \mathtt{zeros}(1,6) \end{pmatrix}. \tag{44}$$

6) Displacement functions:
The displacement functions in the global computational coordinate system η^i

$$\begin{pmatrix} \overset{\eta}{u}_1 \\ \overset{\eta}{u}_2 \\ \overset{\eta}{u}_3 \end{pmatrix} = \mathtt{real}(\mathtt{N} * \mathtt{A}), \tag{45}$$

where

$$N = \begin{pmatrix} v_1 & \mathtt{zeros}(1,343) & \mathtt{zeros}(1,343) \\ \mathtt{zeros}(1,343) & v_2 & \mathtt{zeros}(1,343) \\ \mathtt{zeros}(1,343) & \mathtt{zeros}(1,343) & v_3 \end{pmatrix}, \tag{46}$$

with v_1, v_2, v_3 defined by (31). Results are demonstrated in the global Cartesian coordinate system y^i

$$\overset{y}{u}_j = \frac{\partial \eta^i}{\partial y^j} \overset{\eta}{u}_i \,. \tag{47}$$

C. Results

The results are demonstrated for three different types of loading by internal pressures. The first set (Fig. 11) shows the response to the loading by pressure p_2 only, see Fig. 9. The second set (Fig. 12) shows the response to the loading by pressure p_1 only, see Fig. 9. The third set (Fig. 13) shows the response to the loading by pressures p_1 and p_2 together, $p_2 = 2p_1$.

IV. Conclusion

This report presents the new results of our work. We have introduced the closed anisotropic elastic models whose geometry and cross-section are motivated by human heart shape. Entire deformation analysis was described for one of these models and results for three different types of loading are depicted in the final part of this report.

We are going to use this presented geometric model of human heart in the next step of our planned work to perform viscoelasto dynamic analysis of the heart.

Acknowledgment

The authors would like to thank MSM 6840770012 and GACR 101/08/H068.

References

[1] L. Jiran, K. Doubrava, M. Stefan, and T. Mareš. Analysis of the Heart Motivated Anisotropic Elastic Tube. *Bulletin of Applied Mechanics*, 6(23):57–65, 10 2010.

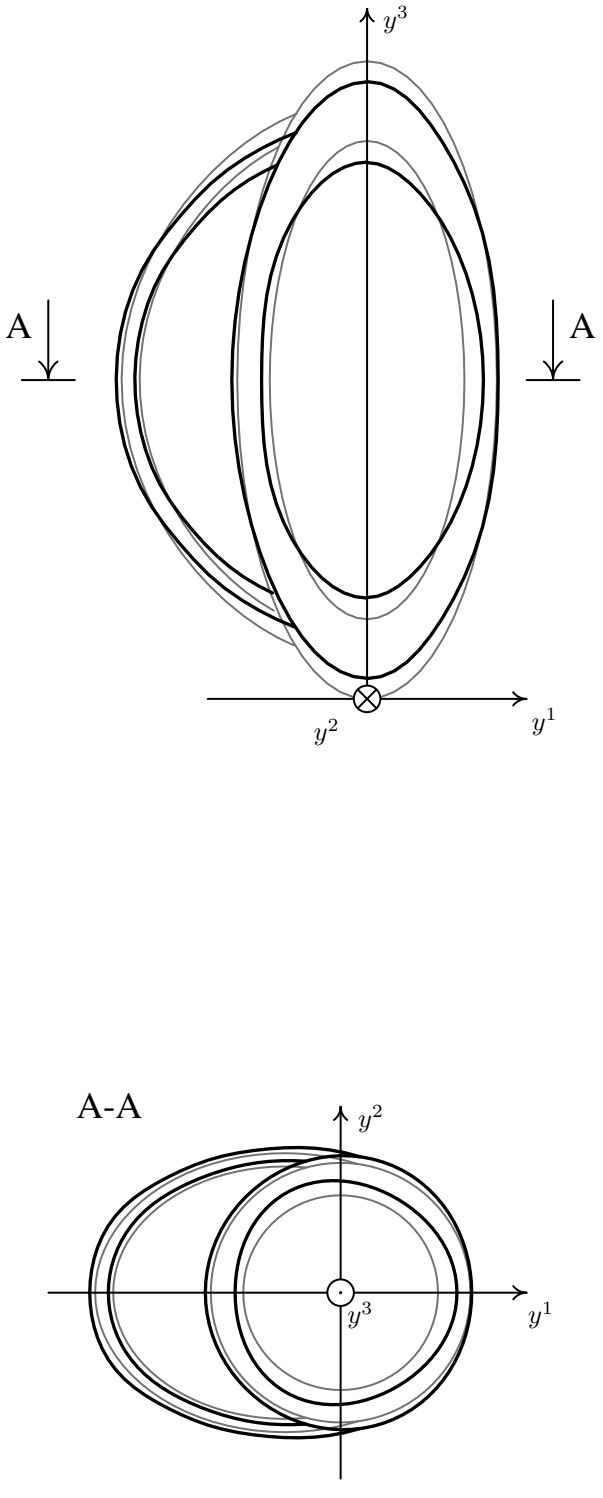

Fig. 11. Response to the loading by p_2.

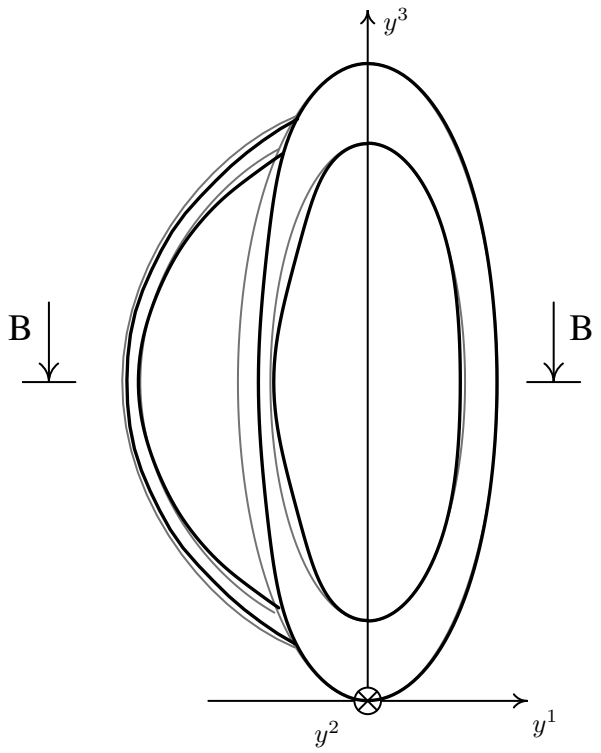

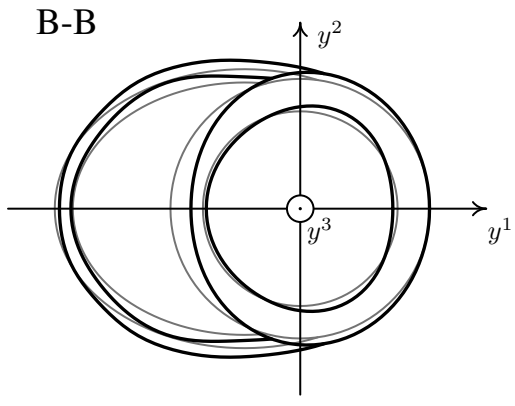

Fig. 12. Response to the loading by p_1.

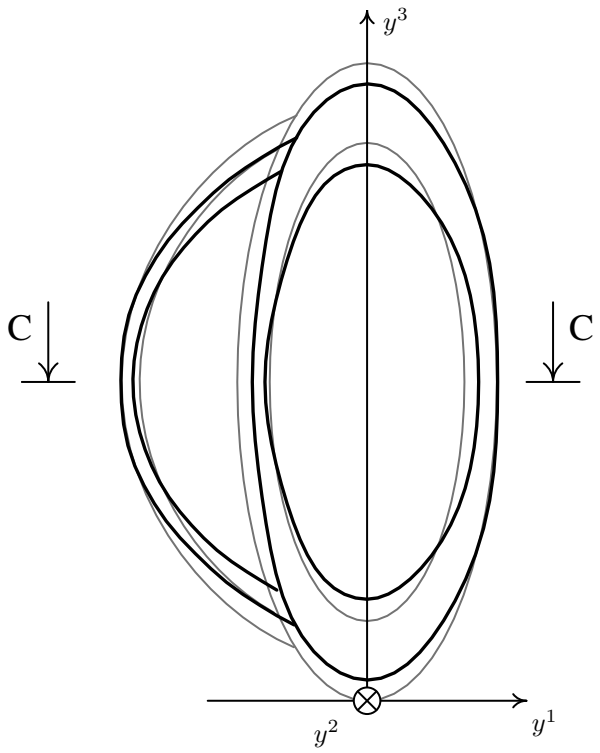

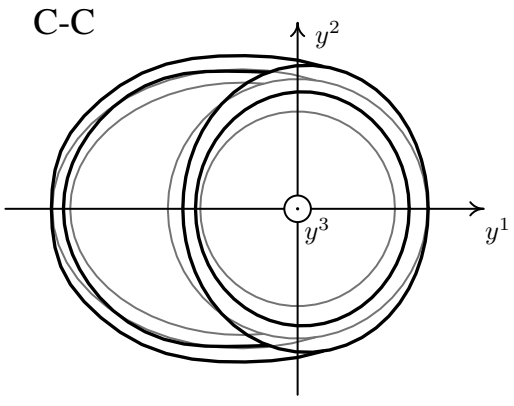

Fig. 13. Response to the loading by p_1 and p_2, $p_2 = 2p_1$.